Continuous Monitoring of the Lunar or Martian Subsurface Using On-Board Pattern Recognition and Neural Processing of Rover Geophysical Data

J. W. McGill, C. E. Glass, and B. K. Sternberg
Department of Mining and Geological Engineering
The University of Arizona

A proposal submitted by the Laboratory for Advanced Subsurface Imaging (LASI) to the Center for Utilization of Local Planetary Resources entitled "Continuous Monitoring of the Lunar or Martian Subsurface Using On-Board Pattern Recognition and Neural Processing of Rover Geophysical Data" includes research using the ground-penetrating radar (GPR) and seismic systems. The ultimate goal of this research is to create an extraterrestrial unmanned system for subsurface mapping and exploration. Neural networks are to be used to recognize anomalies in the profiles that correspond to potentially exploitable subsurface features.

The GPR signal patterns are analogous to seismic patterns, and the preprocessing techniques are likewise identical. Hence, our preliminary research focus on GPR systems will be directly applicable to seismic systems once such systems can be designed for continuous operation. The original GPR profile may be very complex due to electrical behavior of the background, targets, and antennas, much as the seismic record is made complex by multiple reflections, ghosting, and ringing. Because the format of the GPR data is similar to the format of seismic data, seismic processing software may be applied to GPR data to help enhance the data. A neural network may then be trained to more accurately identify anomalies from the processed record than from the original record.

Advantages to Designing a GPR System

Earth-based radar has been used to determine statistical descriptions of the surface and near-subsurface properties of the Moon and the near planets since the development of radar during World War II (Evans et al. 1968). The deductions of the lunar surface and subsurface from Earth-based radar were verified by experiments carried out by the Apollo missions. Therefore, it is believed that radar measurements of the planets should give reliable estimates for planetary electrical properties. The data from these measurements can be used in designing the proper parameters for an extraterrestrial radar survey system.

GPR is sensitive to the water content of the soils being surveyed. Although water creates good radar reflectors, it also attenuates the transmitted and reflected signals, seriously limiting the depth of investigation of the system. Lunar samples have shown

that the soils have the electrical properties of very good dielectric insulators and have an absence of water. The mean atmospheric pressure and temperature of Mars is far below the triple point of water. Venus has surface temperatures and pressures that are far above the critical point of water. Therefore, water will most likely not contribute to the dielectric properties of these planets (Strangway and Olhoeft 1977). It may be expected that GPR will have an excellent depth of penetration, as well as excellent responses to changes between the dielectric constants of subsurface anomalies and the dielectric constants of the surrounding regolith.

Past Lunar Experiments

Lunar profiles were collected by the Apollo 17 astronauts during the surface electrical properties (SEP) experiment in December 1972. SEP was designed to perform the same functions through interferometry that LASI is trying to perform with GPR, i.e., to detect electrical layering, discrete scattering bodies, and the possible presence of water.

A single model to fit all of the SEP data was not found. Resolution was not great enough to detect near-surface anomalies (Strangway et al. 1975). High-frequency GPR has excellent resolution, and GPR's use of pulses instead of continuous waves facilitates interpretation as long as the profiles are not saturated with noise. Conclusions and results from the SEP experiment should be utilized in the planning and construction of a new extraterrestrial electrical experiment. LASI is presently corresponding with Dr. Peter Annan, who was a co-scientist of the SEP experiment and is a developer of digital GPR systems, for insight into developing the extraterrestrial GPR system.

Potential Earth Test Sites

The closest terrestrial approximations of the lunar and near-planet surface conditions are the Sahara Desert and the Poles, where there is either very little water present in the wind-blown sands or the water is frozen and therefore not detrimental to the radar wave. The space shuttle Columbia performed shuttle imaging radar (SIR-A) experiments over the Eastern Sahara in November 1981. Although very high frequencies were used, calculated depths of penetration of dry sand based on laboratory experiments were greater than 5 m, while field studies have verified depths greater than 2 m (McCauley et al. 1982). The University of Munster and the Free University of Berlin have worked together with the General Petroleum Company of Egypt in using GPR to survey the groundwater system of Southern Egypt. Frequencies of 20 and 50 MHz were used to survey depths up to 45 m (Blindow et al. 1987). The extremely dry sands are similar to conditions that will be found on lunar and Martian

surfaces. Comparisons between shuttle radar and surface radar over the Sahara sites should help in the design of GPR systems that will work on the surface of planets that already have high-frequency radar data.

Processing Radar Data

Current research at LASI includes using commercial seismic data-processing software to enhance the radar returns. MIRA, from the Oklahoma Seismic Corporation, is the software being used presently. The following figures demonstrate what may be done with the data to make anomalies more easily recognizable for neural networks.

Figure 3.11 is the standard printout from the profile recorder purchased as part of a commercial GPR system from Geophysical Survey Systems, Inc. This profile was taken over a pipe buried at The University of Arizona School Mine GPR test site. The pipe is buried at a known depth of 38 cm. The sweep rate of the recorder was set at 16 scans per second and the 500 MHz antenna was pulled over the pipe at a slow walking pace. Marks on the record were made at meter intervals along the profile line.

After recording the analog signals, another traverse was made with a Tektronix scope digitizing the analog signal, the results of which are shown in Figure 3.12. Traces were recorded every 10 cm along the profile line. Trace 1 on the digital record corresponds to the first mark on the left of Figure 3.11, trace 10 corresponds to the second, trace 20 to the third, and so on. By having the antenna fixed in one position during a sampling, a real-time stacking may be performed by the Tektronix scope in order for coherent signals to add and incoherent noise to cancel, thereby increasing the signal-to-noise ratio.

Because the traces have been digitized, computer algorithms may be applied to the traces to enhance the returns. All trace-attribute data of Figures 3.13 to 3.19 are the same data presented as profile traces in Figure 3.12. The basic assumption of MIRA is that any periodic function, such as a GPR trace s(t) can be considered as the real part of a complex function S(t), which has both a real part and an imaginary part:

$$S(t) = s(t) + is^*(t) .$$

$s^*(t)$ can be calculated from the trace s(t) with a Hilbert Transform. Any complex number can also be written as

$$S(t) = A(t)e^{i\theta(t)}$$

so that

$$A(t)e^{i\theta(t)} = s(t) + is^*(t) ,$$

where A(t) is called the instantaneous amplitude and

$\theta(t)$ is called the instantaneous phase.

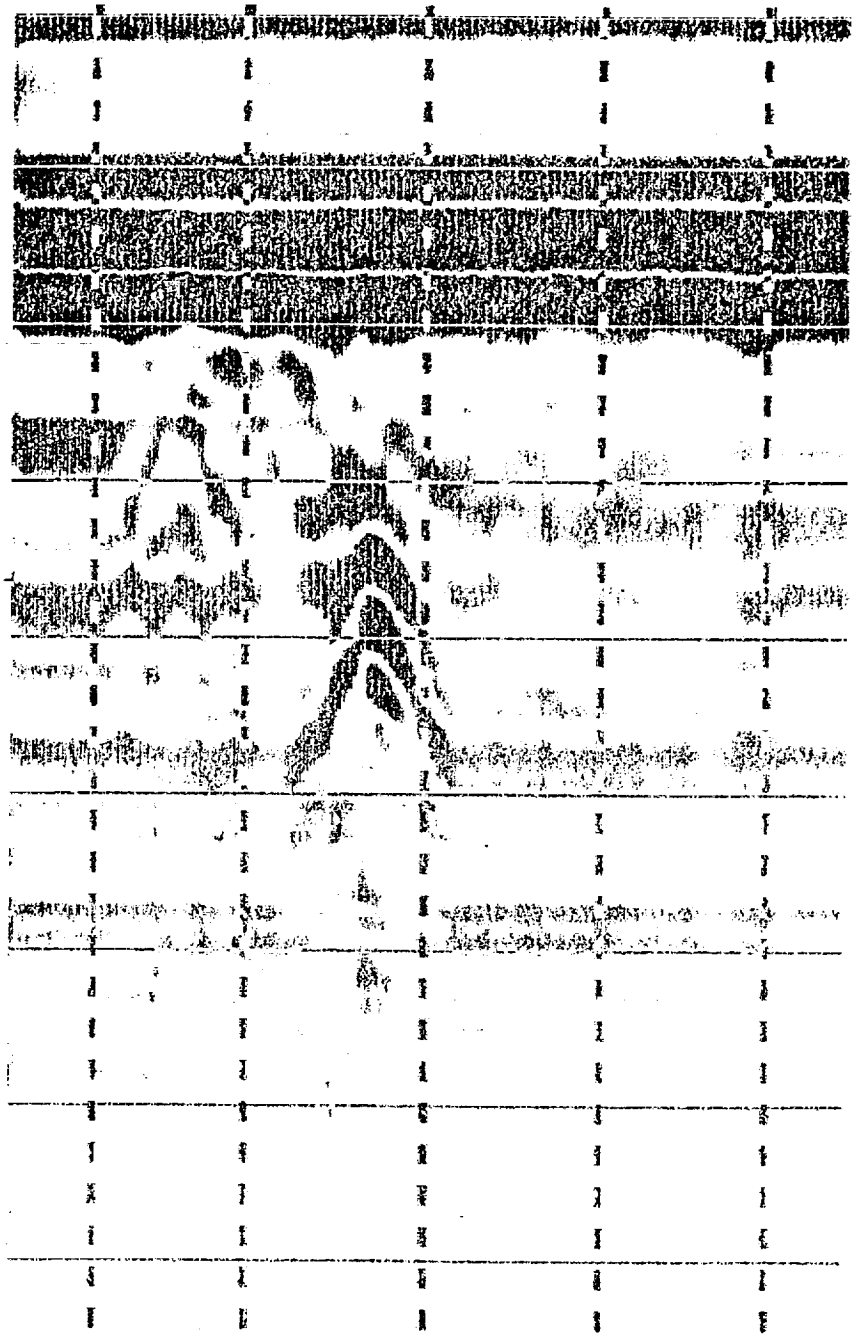

Figure 3.11 Output of analog profile over pipe buried 38 cm deep. Vertical axis is time (2.5 nsecs/div.); horizontal axis is distance (1 m/div.).

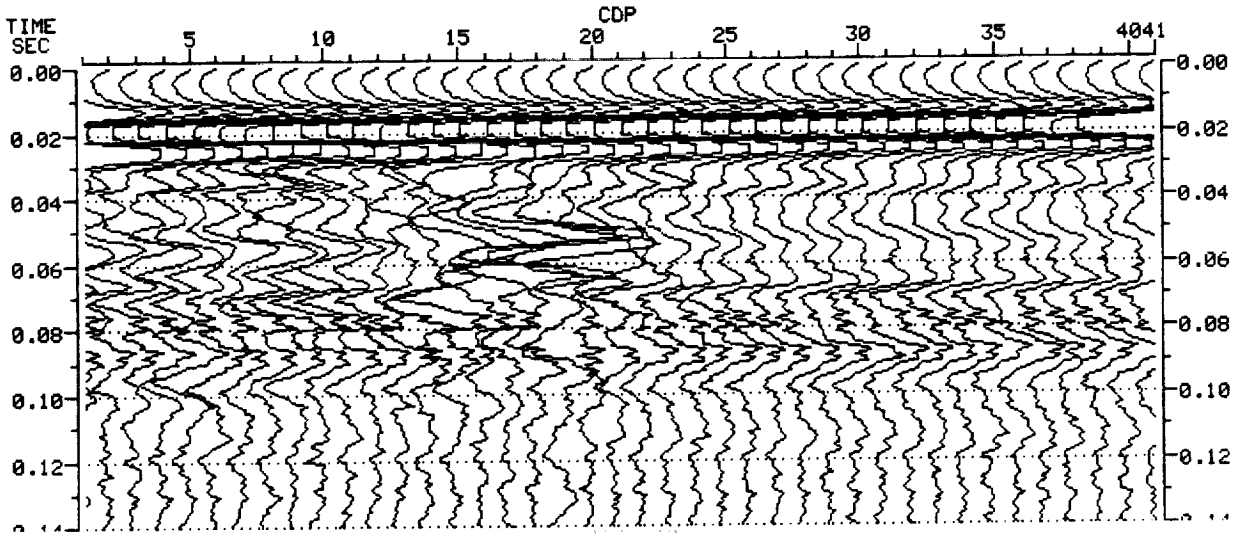

Figure 3.12 Output of digitized profile of same target as that of Figure 3.11. Each CDP represents a 10-cm shift such that 10 CDP's equal a 1-m horizontal shift.

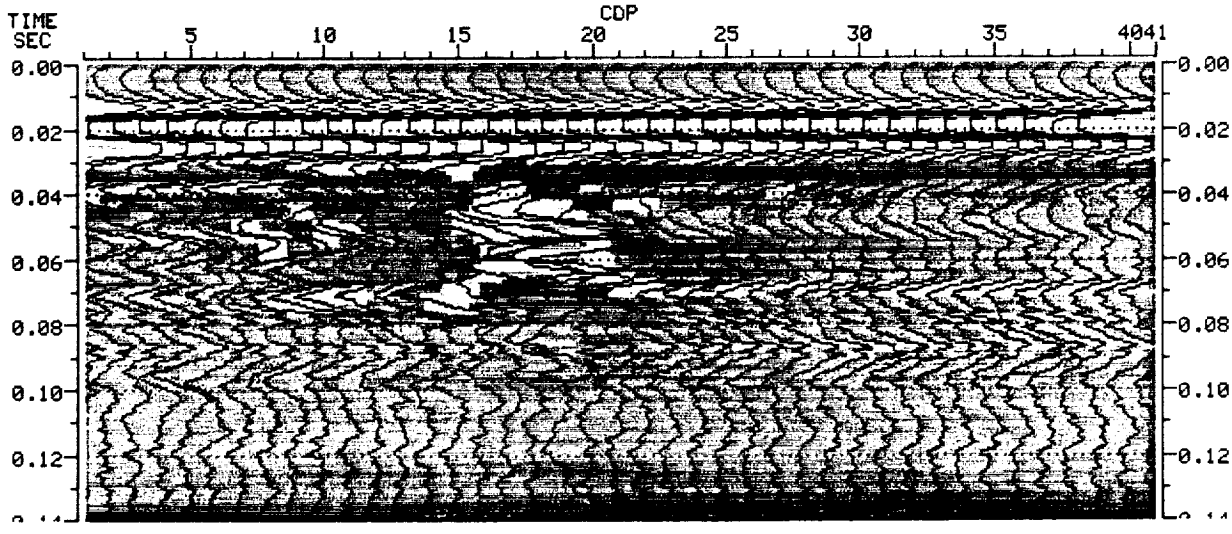

Figure 3.13 Instantaneous amplitude from digitized traces of Figure 3.12. Traces were left on the plot for reference.

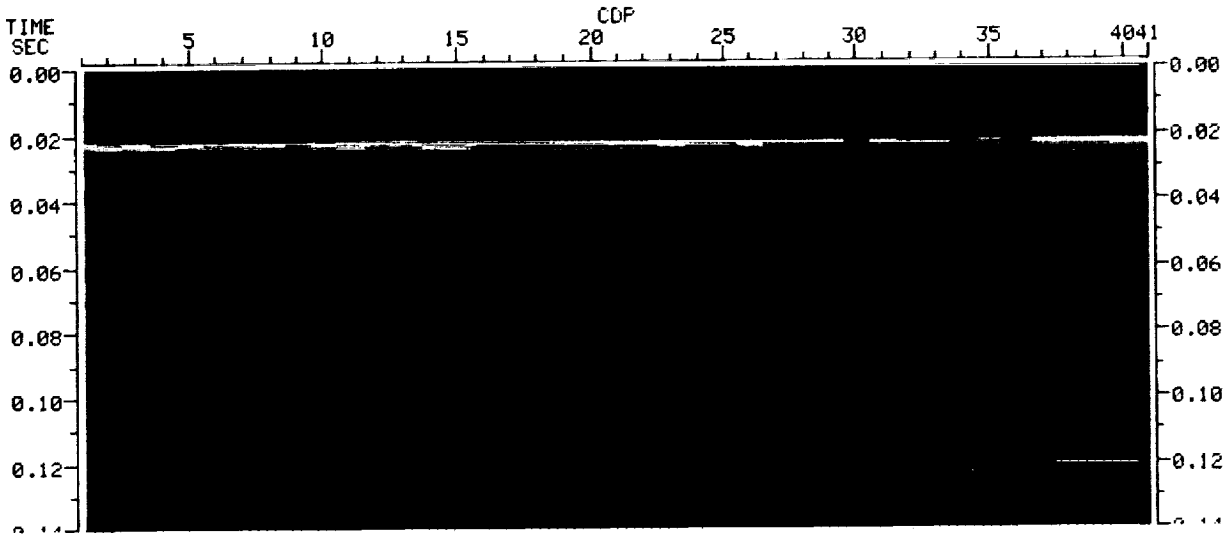

Figure 3.14 Instantaneous power from digitized traces of Figure 3.12.

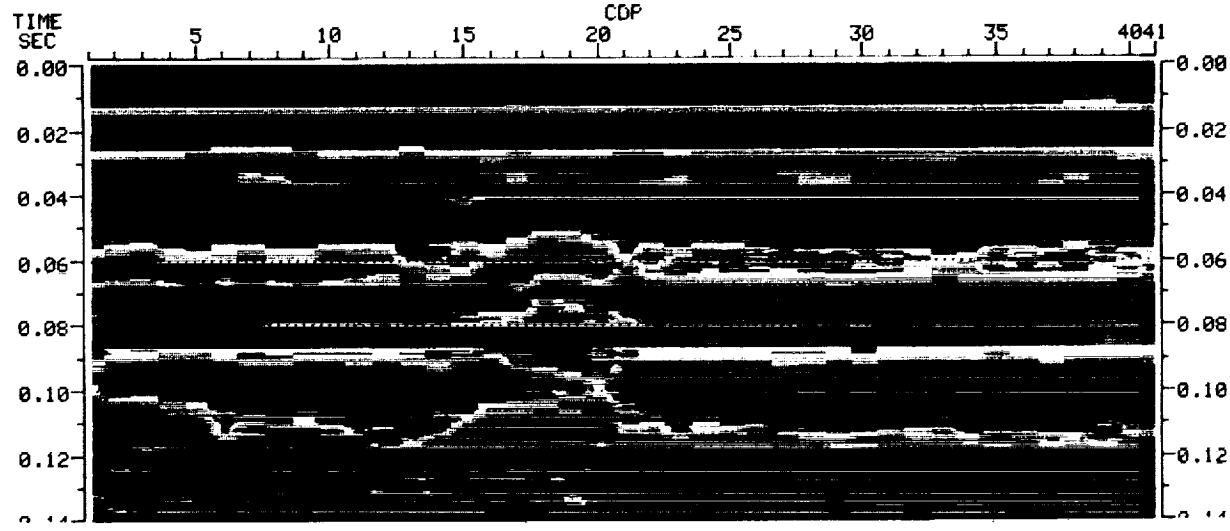

Figure 3.15 Instantaneous phase from digitized traces of Figure 3.12.

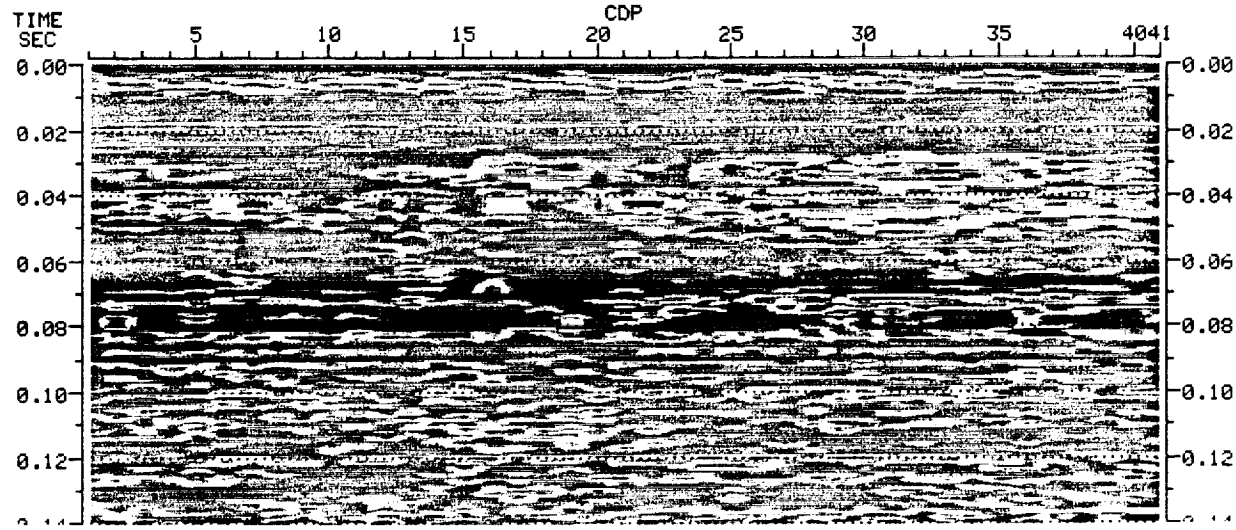

Figure 3.16 Instantaneous frequency from digitized traces of Figure 3.12.

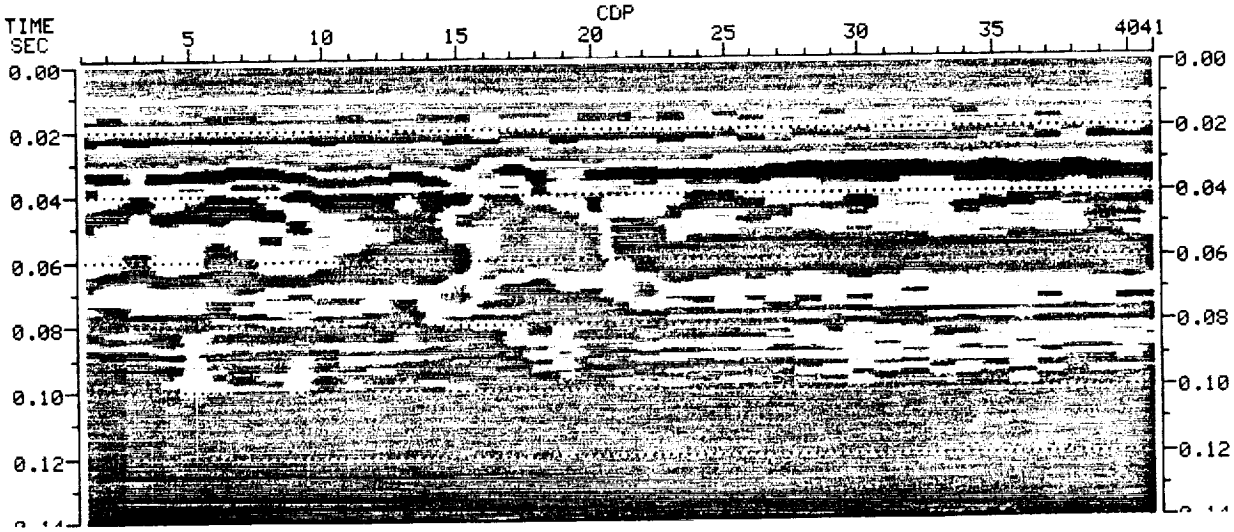

Figure 3.17 Reflection strength from digitized traces of Figure 3.12.

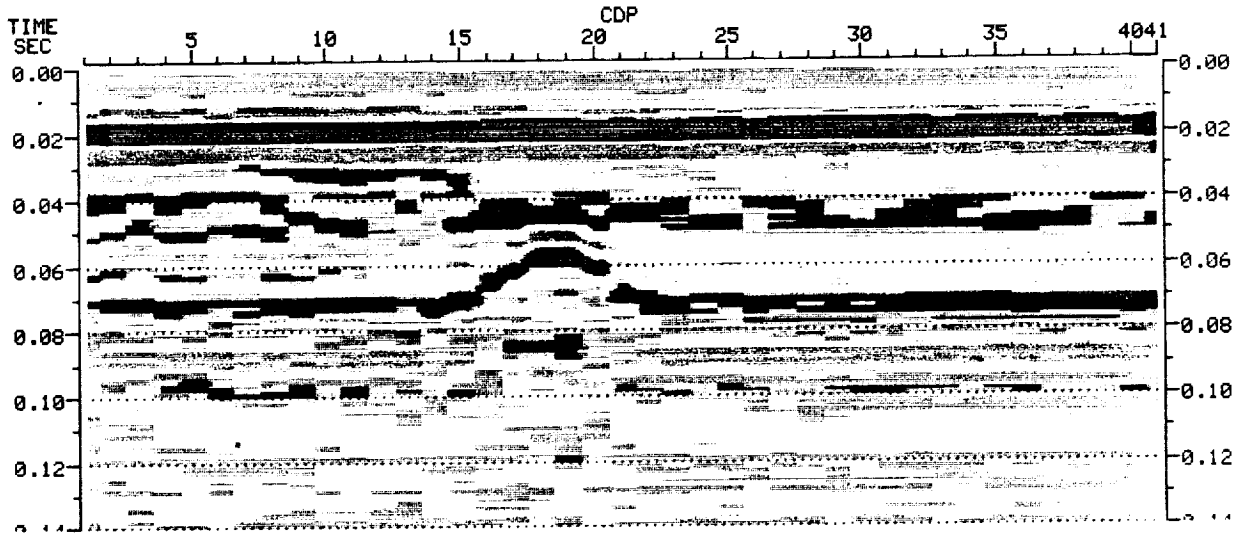

Figure 3.18 Real polarity from digitized traces of Figure 3.12.

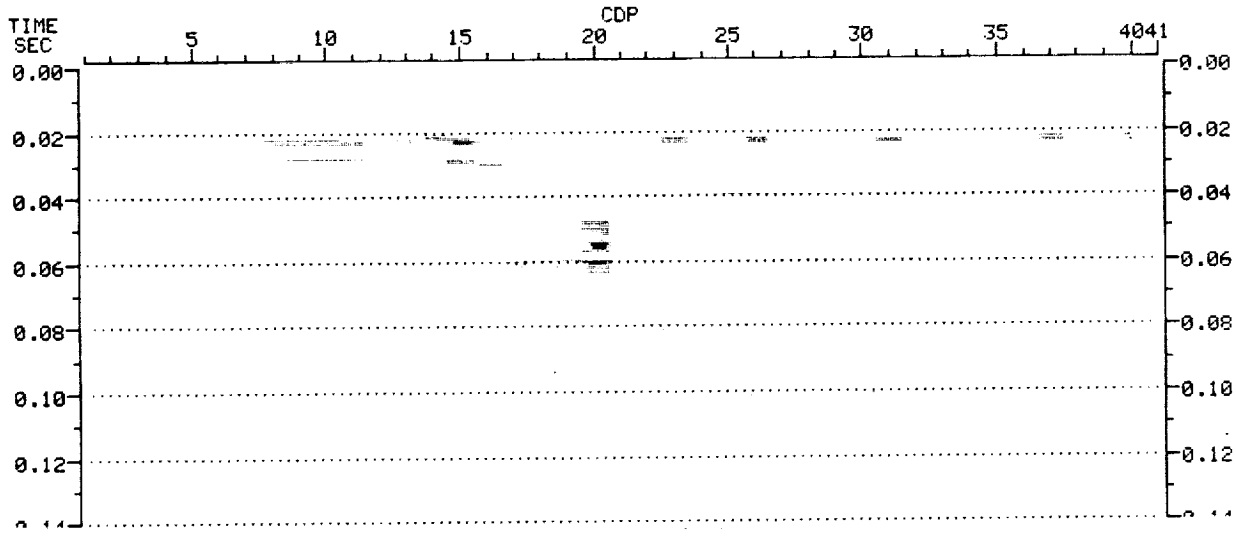

Figure 3.19 Amplitude-weighted imaginary part of the phase difference of adjacent traces of Figure 3.12.

MIRA uses the instantaneous amplitude and the instantaneous phase to calculate all other attributes. The individual traces are plotted in MIRA by a color spectrum, with low values represented by violet and high values represented by red. Instantaneous amplitude is plotted in Figure 3.13, and instantaneous phase in Figure 3.15.

A few examples of some other attributes calculated by MIRA are given in Figures 3.14 to 3.19. Figure 3.14 is the instantaneous power display that is computed by squaring the instantaneous amplitude. Power displays tend to accentuate high-amplitude events. Figure 3.16 is the instantaneous frequency, which is calculated by taking the time derivative of the instantaneous phase attribute. Figure 3.17 is the reflection strength, or decibel display, which is a normalized logarithmic display of the instantaneous amplitude. This function tends to equalize the low- and high-amplitude events. Figure 3.18 is the real polarity, which is simply a color-coded display of the real seismic trace weighted by its amplitude. Figure 3.19 is an amplitude-sine-phase difference plot created by taking two adjacent traces, calculating the phase difference between them, and then weighting the resulting imaginary part of the phase difference by the instantaneous amplitude.

From these examples, it may be seen that MIRA can be very useful, enhancing the returns from a subsurface feature. However, most features are found with a much lower signal-to-noise ratio that the example shown. The algorithms used by MIRA are not powerful enough to increase the signal-to-noise ratio significantly for many of these features. For this reason, LASI is reformatting the GPR data for a more powerful data-processing package. Routines such as deconvolution, various filters, and migration will be applied to these data to determine which sequence of operations will best increase the signal-to-noise ratio, so that subsurface anomalies will be more distinct from the surrounding background.

Once signal patterns are considered optimal, neural network pattern recognition will be applied to permit rapid recall of pattern associations. Our research on neural network pattern recognition of other EM geophysical patterns has demonstrated, for the first time (see, for example, Poulton et al. 1989), that our pattern recognizers can not only recall known patterns accurately, but can generalize and form abstractions when faced with patterns that are not part of the training suite.

Selected Bibliography

Annan, A. P. and Davis, J. L., 1977, "Radar Range Analysis for Geological Material: Report of Activities," *Geol. Surv. Can. Paper 77-1B*, pp. 117-124.

Blindow, N., Ergenzinger, P., Pahls, H., Scholz, H., and Thyssen, F., 1987, "Continuous Profiling of Subsurface Structures and Groundwater Surface by EMR Methods in Southern Egypt, Subproject B11," pages 575-627 in *Research in Egypt and Sudan, Results of the Special Research Project Arid Areas Period 1984-1987* (E. Klitzsch and E. Schrank, eds.), Verlag von Dietrich Reimer, Berlin.

Daniels, J. J., 1988, "Fundamentals of Ground Penetrating Radar," Department of Geology and Mineralogy, Ohio State University, Columbus.

Elachi, C., Brown, W. E., Cimino, J. B., Dixon, T., Evans, D. L., Ford, J. P. Saunders, R. S., Breed, C., Masursky, H., McCauley, J. F., Schaber, G., Dellwig, L., England, A., MacDonald, H., Martin-Kaye, P., and Sabins, F., 1982, "Shuttle Imaging Radar Experiment," *Science*, Vol. 218, pp. 996-1003.

Evans, J. V. and Hagfors, T., 1968, *Radar Astronomy*, McGraw-Hill Book Company, New York.

McCauley, J. F., Schaber, G. G., Breed, C. S., Grolier, M. J., Haynes, C. V., Issawi, B., Elachi, C., and Blom, R., 1982, "Subsurface Valleys and Geoarchaeology of the Eastern Sahara Revealed by Shuttle Radar," *Science*, Vol. 218, pp. 1004-1020.

McDonald, H. C., 1980, "Techniques and Applications of Imaging Radars," pages 297-336 in *Remote Sensing in Geology* (B. S. Seigal and A. R. Gillespie, eds.), John Wiley and Sons, New York.

McGill, J. W., Sternberg, B. K., and Glass, C. E., 1989, "Applications of Ground Penetrating Radar in Southern Arizona," LASI-89-2, The University of Arizona, Tucson.

Poulton, M. M., Glass, C. E., and Sternberg, B. K., 1989, "Recognizing EM Elipticity Patterns With Neural Networks," *SEG 59th Annual Meeting, Expanded Abstracts*, Vol. 1, EM38, pp. 208-212.

Strangway, D. W., Annan, A. P., Redman, J. D., Rossiter, J. R., and Watts, R. D., 1975, "Electrical Structure at Taurus-Littrow," NASA Techical Publications N-75-16308.

Strangway, D. W. and Olhoeft, G. R., 1977, "Electrical Properties of Planetary Surfaces," *Phil. Trans. Roy. Soc. Lond. A*, Vol. 285, pp. 441-450.